Chemical Science

ROYAL SOCIETY OF CHEMISTRY

EDGE ARTICLE

View Article Online
View Journal | View Issue

Cite this: *Chem. Sci.*, 2025, **16**, 3173

All publication charges for this article have been paid for by the Royal Society of Chemistry

Theoretical study of the *in situ* formation of H_2O_2 by lytic polysaccharide monooxygenases: the reaction mechanism depends on the type of reductant†

Zhanfeng Wang, *[a] Xiaodi Fu,[a] Wenwen Diao,[b] Yao Wu,*[c] Carme Rovira *[de] and Binju Wang *[c]

Received 11th October 2024
Accepted 9th January 2025

DOI: 10.1039/d4sc06906d

rsc.li/chemical-science

Lytic polysaccharide monooxygenases (LPMOs) are a unique group of monocopper enzymes that exhibit remarkable ability to catalyze the oxidative cleavage of recalcitrant carbohydrate substrates, such as cellulose and chitin, by utilizing O_2 or H_2O_2 as the oxygen source. One of the key challenges in understanding the catalytic mechanism of LPMOs lies in deciphering how they activate dioxygen using diverse reductants. To shed light on this intricate process, we conducted in-depth investigations using quantum mechanical/molecular mechanical (QM/MM) metadynamics simulations, molecular dynamics (MD) simulations, and density functional theory (DFT) calculations. Specifically, our study focuses on elucidating the *in situ* formation mechanism of H_2O_2 by LPMOs in the presence of cellobiose dehydrogenase (CDH), a proposed natural reductant of LPMOs. Our findings reveal a proton-coupled electron transfer (PCET) process in generating the Cu(II)-hydroperoxide intermediate from the Cu(II)-superoxide intermediate. Subsequently, a direct proton transfer to the proximal oxygen of Cu(II)-hydroperoxide results in the formation of H_2O_2 and LPMO-Cu(II). Notably, this mechanism significantly differs from the LPMO/ascorbate system, where two hydrogen atom transfer reactions are responsible for generating H_2O_2 and LPMO-Cu(I). Based on our simulations, we propose a catalytic mechanism of LPMO in the presence of CDH and the polysaccharide substrate, which involves competitive binding of the substrate and CDH to the reduced LPMOs. While the CDH-bound LPMOs can activate dioxygen to generate H_2O_2, the substrate-bound LPMOs can employ the H_2O_2 generated from the LPMO/CDH system to perform the peroxygenase reactions of the polysaccharide substrate. Our work not only provides valuable insights into the reductant-dependent mechanisms of O_2 activation in LPMOs but also holds implications for understanding the functions of these enzymes in their natural environment.

1 Introduction

Utilizing abundant and renewable polysaccharides, such as cellulose, starch, and chitin, to produce biofuels and commercial chemicals is highly appealing, serving as a promising solution to address future shortages and environmental threats associated with fossil-based energy and chemicals. However, there is a major obstacle to degrade polysaccharides into smaller units due to their inherent recalcitrance.[1] Lytic polysaccharide monooxygenases (LPMOs), key elements of current commercial enzymatic mixtures for the processing of lignocellulosic biomass,[1–4] have been well known for their roles in boosting degradation of polysaccharides since their identification in 2010.[5]

LPMOs belong to a superfamily of mono-copper enzymes that oxidatively depolymerize polysaccharides through hydroxylation of the C1 or C4 position of the scissile glycosidic bond connecting the sugar units.[6–9] The copper ion in LPMOs is coordinated by two conserved histidine residues, forming a structure known as the "histidine brace" (refer to Fig. 1).[10–12] Mechanistically, LPMOs can activate both O_2 and H_2O_2 (as a cosubstrate) to form an active species, Cu(II)-oxyl ($[CuO]^+$), which is generally believed to be responsible for C4–H/C1–H

[a]*Center for Advanced Materials Research & Faculty of Arts and Sciences, Beijing Normal University, Zhuhai 519087, China. E-mail: zfwang@bnu.edu.cn*

[b]*Oujiang Laboratory (Zhejiang Lab for Regenerative Medicine, Vision and Brain Health), Wenzhou, Zhejiang 325000, China*

[c]*State Key Laboratory of Physical Chemistry of Solid Surfaces and Fujian Provincial Key Laboratory of Theoretical and Computational Chemistry College of Chemistry and Chemical Engineering, Xiamen University, Xiamen 361005, China. E-mail: wuyao@xmu.edu.cn; wangbinju2018@xmu.edu.cn*

[d]*Departament de Química Inorgànica i Orgànica & IQTCUB, Universitat de Barcelona, Martí i Franquès 1, 08028 Barcelona, Spain. E-mail: c.rovira@ub.edu*

[e]*Institució Catalana de Recerca i Estudis Avançats (ICREA), Passeig Lluís Companys, 23, 08010 Barcelona, Spain*

† Electronic supplementary information (ESI) available. See DOI: https://doi.org/10.1039/d4sc06906d

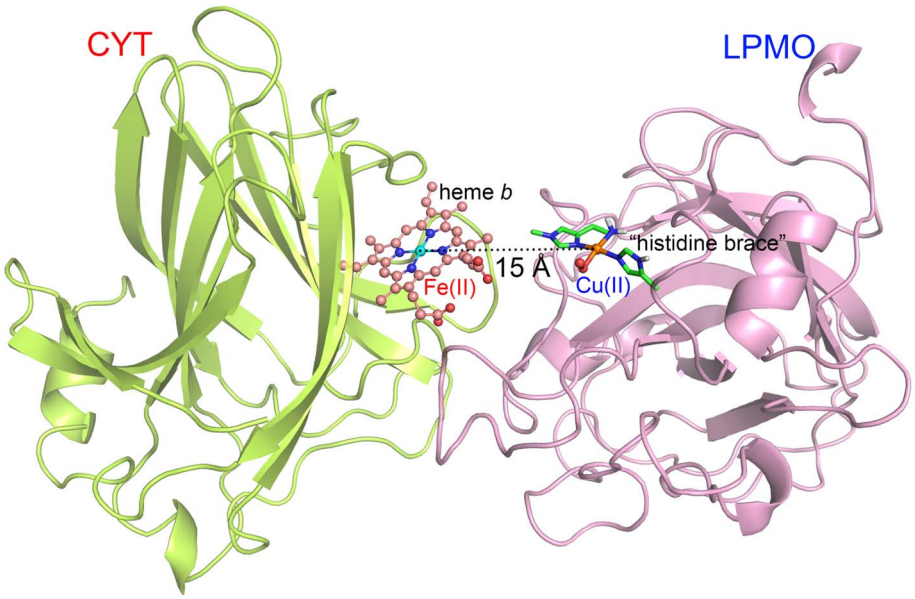

Fig. 1 Interaction complex of LPMO and the CYT domain of CDH. The distance between CYT-Fe and LPMO-Cu is only *ca.* 15 Å, which can guarantee an efficient electron transfer between them.

hydroxylation.[13–21] Initially, LPMOs were characterized as monooxygenases using molecular oxygen as the co-substrate.[5,11,22–25] However, an increasing number of studies supported that LPMOs can also be H_2O_2-dependent peroxygenases.[13,21,26–31] Interestingly, it has been established that substrate-free LPMOs can produce H_2O_2 (oxidase reactivity) through uncoupled turnover when exposed to O_2 and a reducing agent,[32–35] which further complicates the elucidation of their molecular mechanism. Recently, the H_2O_2 production capability of LPMOs has been harnessed for fueling enzyme cascade reactions.[36,37] Therefore, gaining an in-depth understanding of their oxidase reactivity is essential for elucidating the atomic details of LPMOs' catalytic mechanism and for harnessing their potential applications.

The molecular mechanism of *in situ* formation of H_2O_2 by LPMOs has been theoretically studied in several studies.[20,38–40] Scheme 1 provides an overview of the possible catalytic pathways for the formation of active species *via* the O_2-dependent activity. In the resting state, the copper ion is in the Cu(II) state. It is well established that the Cu(II) center requires a priming reduction for subsequent activation of O_2 or H_2O_2 (path a).[6] This reduction can be facilitated by a reducing agent such as ascorbate or the enzyme cellobiose dehydrogenase (CDH).[41,42] While ascorbate is suitable for homogeneous LPMO preparations, CDH ensures a specific and efficient electron transfer (ET) with LPMOs, making it more suitable for fermentation samples.[32,41] Additionally, the use of CDH enables a kinetically controlled supply of electrons, providing advantages over small molecule reductants.[43] Starting from the reduced Cu(I) ion, the binding of O_2 to the active site leads to the formation of the Cu(II)-superoxide ($[CuO_2]^+$) intermediate (path b).[24] The Cu(II)-superoxide species then accepts a proton and an electron (a hydrogen atom), resulting in the formation of the Cu(II)-hydroperoxide ($[CuO_2H]^+$) species (path c). The superoxide and hydroperoxide species have been captured in a neutron crystallography study, confirming the formation and stability of them.[44] From the hydroperoxide species, several possible pathways have been suggested, depending on the oxygen atom being subsequently protonated. A QM/MM study by Hedegård and Ryde suggested that protonation of the distal oxygen atom of the Cu(II)-hydroperoxide species leads to the cleavage of the O–O bond, the dissociation of a water molecule, and the formation of the Cu(III)-oxyl species (path d).[39] Subsequent one-electron reduction of Cu(III)-oxyl results in the formation of the

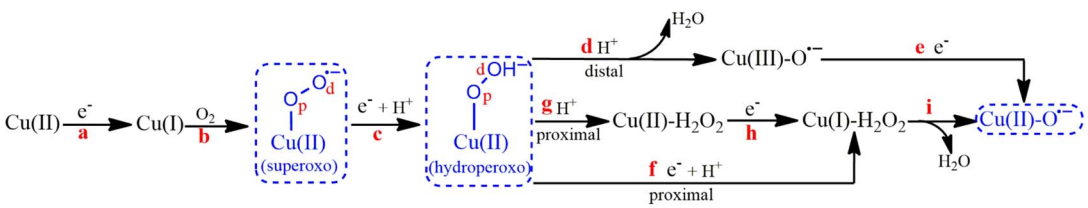

Scheme 1 Possible catalytic pathways for the formation of active species Cu(II)-oxyl *via* the O_2-dependent activity in LPMOs. The proximal (p) and distal (d) oxygen atoms in Cu(II)-superoxide and Cu(II)-hydroperoxide species are labeled for clarity.

active species Cu(II)-oxyl (path e).[39] In contrast, a QM/MM study by Wang *et al.* suggested that protonation at the distal oxygen atom (path d) is not feasible and instead protonation occurs at the proximal position, coupled with an electron transfer from ascorbate to the copper ion (path f), yielding the Cu(I)–H_2O_2 complex.[38] It is noteworthy that the energetic features depend on the functional used for the QM region and the choice of the QM region itself.[39,40] A very recent QM/MM study by Hedegård and co-workers using a large QM region also excluded the feasibility of path d.[40] Alternatively, the proton may transfer to the proximal oxygen atom of the Cu(II)-hydroperoxide species, forming the Cu(II)–H_2O_2 complex (path g),[20] and subsequently one-electron reduction yields the Cu(I)–H_2O_2 complex (path h). From there, Cu(I)–H_2O_2 can readily evolve into the active species Cu(II)-oxyl with the dissociation of one water molecule (path i).[19,20] Notably, the reaction of reduced LPMO with H_2O_2 in the absence of a substrate or excessive H_2O_2 can lead to enzyme damage and eventually inactivation.[13,45–48]

It is worth noting that a consensus regarding the O_2 activation mechanism by LPMOs has not been reached. The studies conducted by Hedegård and colleagues considered the involved ET process in an implicit way,[20,39] while the work by Wang *et al.* explicitly accounted for it using the ascorbate monoanion ($AscH^-$) as the reductant.[38] Ascorbate is the most extensively studied small molecule reductant, whereas CDH is the enzymatic reductant considered as the natural electron donor for LPMOs and is more suitable for fermentation samples.[32,41,49] It has been well established that the N-terminal heme b-containing cytochrome (CYT) domain of CDH serves as the electron donor and interacts directly with LPMOs.[50,51] Additionally, it is well known that different reductants lead to different LPMO activities,[41,52] which may be attributed to variations in the H_2O_2 generation rate.[53–57] Mechanistically, $AscH^-$ possesses an active hydrogen atom capable of providing an electron and a proton simultaneously.[38] In contrast, the reduced CYT can only supply electrons. Consequently, the use of CDH as a reducing agent is expected to result in a different O_2 activation mechanism. In this study, we employ a combination of MD simulations and QM/MM MD simulations to (i) uncover the O_2 activation mechanism by LPMOs when CDH is utilized as the reductant, (ii) compare this mechanism with the LPMO/ascorbate system and elucidate the reductant-dependent reactivity of LPMOs, and (iii) provide insights into the connection between O_2-dependent and H_2O_2-dependent pathways.

2 Computational methods

2.1. System setup

The model system used in this study includes only the CYT domain of CDH and the LPMO enzyme. This choice, which lowers the computational cost, is supported by experimental evidence demonstrating that the reduced CYT domain is responsible for LPMO reduction.[50] The LPMO structure was obtained from a high-resolution X-ray structure of *Lentinus similis* (*Ls*AA9, PDB ID: 5ACF),[58] while the CYT domain was taken from the structure of *Neurospora crassa* CDH (PDB ID: 4QI7).[50] The interaction complex between LPMO and CYT (Fig. 1) was taken from our previous study.[59] The model was initially obtained by protein–protein docking *via* the online program "Z-dock" and subsequently optimized by MD simulations. Based on the interaction complex, two systems, namely CYT-Fe(II) + LPMO-Cu(II)-superoxide (system I) and CYT-Fe(II) + LPMO-Cu(II)-hydroperoxide (system II), were constructed to investigate the two proton transfer (PT) processes involved in the O_2 activation process. The metal-containing active sites of both LPMO and CYT, including LPMO-Cu(II)-superoxide, LPMO-Cu(II)-hydroperoxide, and CYT-Fe(II), were parameterized using the "MCPB.py" tool of AmberTools18.[60,61] The Amber ff14SB force field was applied for the normal protein residues.[62] The protonation states of titratable residues (His, Asp, and Glu) were consistent with our previous study,[59] with the exception of histidine 147, which was doubly protonated to supply a proton during the activation process of O_2 (more discussion of the protonation sate of His147 can be found in the Results and discussion section). Counter ions were added to neutralize the total charge of the system, which was solvated in a rectangular box of TIP3P waters extending up to a minimum cutoff of 16 Å from the protein surface.

2.2. Classical molecular dynamics (MD) simulations

The built systems were first minimized keeping the enzymes fixed, whereas solvent molecules and ions are allowed to move, followed by a full minimization of the whole system with a combination of steepest descent and conjugate gradient methods. Afterwards, each system was gradually heated from 0 to 300 K over 300 ps with a weak restraint of 25 kcal mol^{-1} $Å^{-2}$ on the protein atoms in the canonical ensemble. Subsequently, a 1 ns density equilibration (NPT) simulation was performed under an isothermal-isobaric Langevin thermostat[63] and Berendsen barostat[64] with a collision frequency of 2 ps^{-1} and a pressure relaxation time of 1 ps at a target temperature of 300 K and target pressure of 1.0 atm to achieve a uniform density. Following this, all restraints were removed, and each system was further equilibrated for 3 ns under the NPT ensemble. Finally, three replicas of 100 ns production simulations were performed for each system using different initial velocities. During all MD simulations, covalent bonds containing hydrogen atoms were constrained using the SHAKE algorithm,[65] and an integration step of 2 fs was used. Nonbonded interactions were treated with the Particle Mesh Ewald method,[66] with a cutoff set at 10 Å. All MD simulations were performed with the GPU version of the Amber 18 package.[67–69]

2.3. Constant pH MD simulations

Constant pH MD simulations using discrete protonation states in explicit solvent were performed in system II to determine the fraction of different protonation states of His147 at different pH,[70] which is suggested to act as a proton supplier in this study and several others.[34,39,71,72] The method involves standard MD simulations being propagated in explicit solvent and protonation state changes being attempted in implicit solvent at fixed intervals. Eight 100 ns constant pH MD simulations were carried out spanning the pH range from 4.0 to 7.5 at 0.5 pH-unit intervals. Protonation state changes were attempted every 200 fs

for all constant pH MD simulations. The solvent relaxation time was set to 200 fs as suggested by Swails *et al.*[70]

2.4. QM/MM MD and metadynamics simulations

One representative snapshot extracted from the classical MD trajectories of each system was used for the subsequent QM/MM MD simulations, in which a hydrogen bond between doubly-protonated His147 and Gln162 is formed to ensure an efficient PT. All QM/MM MD simulations were performed with the CP2K package (2022.2 version),[73] which combines the QM program QUICKSTEP[74] and the MM driver FIST. A real space multigrid technique is used to compute the electrostatic coupling between the QM and MM regions.[75,76] The QM region included the active site of LPMO, the reduced heme b cofactor, and several water molecules between them (refer to Fig. S1A and B† for the QM region of system I and system II, respectively). Specifically, the LPMO part consisted of the Cu cofactor, Hic1 residue, and the side chains of residues His78, His147, Gln162, and Tyr164, while the CYT part contained the heme b cofactor and the side chains of two residues that coordinate to the iron of heme, namely Met74 and His176. The remaining atoms were treated at the molecular mechanics (MM) level using the same force-field as in the classical MD simulations, whereas the dangling bonds between the QM and the MM regions were capped with hydrogen atoms. The QM region was described at the DFT(B3LYP-D3) level, using a dual basis set of Gaussian and plane-wave (GPW) formalism.[74] The Gaussian double-ζ valence polarized (DZVP) basis set was used to expand the wave function,[77] converging the electron density employing an auxiliary plane-wave basis set with a density cut-off of 360 Ry, along with Geodecker-Teter-Hutter (GTH) pseudopotentials.[78,79] To accelerate the calculation of the Hartree–Fock exchange within B3LYP, the auxiliary density matrix method (ADMM) was used.[80] All QM/MM MD simulations were performed in the NVT ensemble using an integration time step of 0.5 fs. The systems were first equilibrated without any restraint for 1.5 ps. Then, the metadynamics method[81,82] was used to explore the PT and possibly involved ET processes. The collective variable (CV) was defined as the distance between the proton of His147 (H1) and the distal oxygen atom (O2) for the first PT process, while the difference distance between the H1 atom and the proximal oxygen (O1) atom and between the H1 atom and N1 atom of His147 was used as the CV for the second PT process (refer to Fig. S2†). The width of the Gaussian-shaped potential hills was taken between 0.1 and 0.2 Å. The Gaussian height was set to 0.6 kcal mol^{-1}, while the time deposition interval between two consecutive Gaussians was set to 10 fs. The first re-crossing criterion, as recommended for chemical reactions, was used.[83]

Additional details regarding static QM/MM scanning calculations and small QM model calculations can be found in the ESI Methods section of the ESI.†

3 Results and discussion

3.1. The potential role of His147 as a proton supplier

As alluded to above, the activation of O_2 requires two electrons and two protons. The electrons needed during dioxygen activation are supplied by the reduced CYT domain of CDH in this study, one at a time. The electron transfer (ET) efficiency between CYT and LPMO depends on the distance between the heme-Fe of CYT and the Cu ion of LPMO. In a prior study, we already obtained the interaction complex of CYT and LPMO using a combination of protein–protein docking calculations and classical MD simulations, showing that the distance between heme-Fe and LPMO-Cu is as short as *ca.* 15 Å (Fig. 1), enabling an efficient ET.[59] For the PT reactions, it is clear that the proton acceptors are the Cu(II)-superoxide and the Cu(II)-hydroperoxide species for the first and the second PT, respectively. However, the identity of the proton source is still a matter of debate.[34,38,39,44,71,72,84] A second-sphere histidine residue, His147, has been suggested as a potential proton donor by some experimental studies[34,71,72] and theoretical studies.[39,85] However, refinement of crystal structures (obtained at 100 K) indicated that this residue is in singly-protonated form even under acidic conditions due to the dimeric packing of enzymes.[44,84] Therefore, it is important to investigate the protonation state of this residue under more biologically relevant conditions.

Constant pH MD simulations[70] are performed to determine the fraction of the doubly-protonated form of His147 at different pH values ranging from 4.0 to 7.5 under 300 K, which is shown in Fig. 2. It is seen that in solution the doubly-protonated form is predominant when pH ≤ 5.5. At pH 6, the doubly-protonated form still accounts for 36%. It is noteworthy that the optimal condition for most LPMOs (including the one used in this study) is slightly acidic[85–87] and the best performance of the LPMO + CDH system was achieved at pH 6.0.[41] Besides, the recommended pH range of one of the most popular commercial LPMO-containing cellulose-degrading enzyme cocktails is also slightly acidic, pH 5.0–5.5, for the best performance. Therefore, the condition of pH ≤ 6 is more relevant for LPMOs, under which the formation of the doubly-protonated form of His147 is a high-probability event. Consistent with a recent theoretical study,[85] our simulations show a correlation

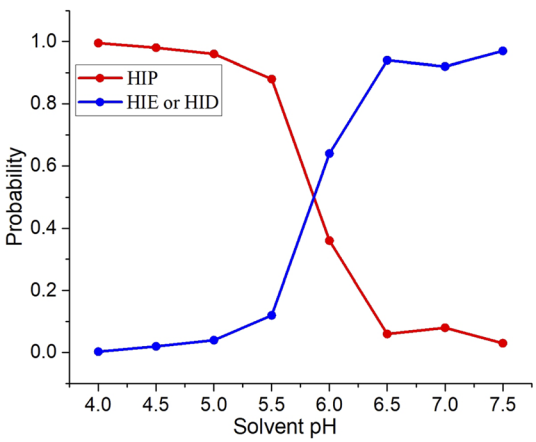

Fig. 2 Probability of different protonation forms of His147 under different solvent pH estimated with constant pH MD simulations. The fraction of the doubly-protonated form (HIP) is shown with red dots, while the fraction of the singly-protonated form, either HIE (epsilon tautomer) or HID (delta tautomer), is shown with blue dots.

between the protonation state and the conformation of His147. For the doubly protonated form, it adopts predominantly a solvent-exposed "outward" conformation, which is further away from the active site (Fig. S3†). The movement of this residue between bulk solvent and the active site may facilitate proton transfers to the active-site pocket, as suggested by Isaksen *et al.*[85]

Next, the potential role of the doubly protonated His147 residue as a proton supplier during the activation process of O_2 is investigated with classical MD simulations. Regardless of the protonation state of the copper-oxide species, *i.e.*, Cu(II)-superoxide and Cu(II)-hydroperoxide, the distance between the electron donor (CYT-Fe(II)) and acceptor (LPMO-Cu(II)) remains within 16 Å (see Fig. S4 and S5† for the time evolution of the Fe–Cu distance during classical MD simulations in the Cu(II)-superoxide and Cu(II)-hydroperoxide system, respectively), which is favourable for efficient ET.[88] In the case of the Cu(II)-superoxide system (Fig. 3A), no direct H-bond is observed between His147 and the distal O2 atom during MD simulations. The distance between His147 and the distal O2 atom is approximately 8 Å for about four-fifths of the total simulation time (middle panel of Fig. 3A and S6†). Instead of forming a H-bond with Cu(II)-superoxide species, His147 is found to form a weak H-bond with the carbonyl group of the side chain of residue Gln162 (refer to Fig. 3A and S7†). This H-bond maintains a distance about 4 Å between H1 of His147 and the distal O2 atom. Similarly, in the case of Cu(II)-hydroperoxide (Fig. 3B), His147 forms a H-bond with the side chain of Gln162 (right panel of Fig. 3B and S8†), which is more stable compared to the Cu(II)-superoxide system. Due to the formation of this H-bond, the distance between His147 and the proximal oxygen atom (O1) of Cu(II)-hydroperoxide remains at around 3.0 Å for most of the simulation time (middle panel of Fig. 3B and S9†). Overall, our MD simulation results indicate that His147 could exist as a doubly-protonated form and serve as a proton supplier under LPMOs' working conditions, yet no direct H-bond forms between His147 and the proton destination copper-oxide species.

3.2. Formation of Cu(II)-hydroperoxide from Cu(II)-superoxide involves PCET

Most of the previous studies agree on the formation of Cu(II)-hydroperoxide species during the activation process of dioxygen. There is one exception worth mentioning, where the superoxide was suggested to react with a water molecule, leading to the formation of Cu(II)–OH and release of hydrosuperoxide, which may further evolve to H_2O_2 in solution.[23] However, our QM scanning calculations show that dissociation of superoxide is highly thermodynamically unfavourable and no proton transfer from the water ligand to the dissociated superoxide is observed (Fig. S10†), which is consistent with a previous computational study.[20] Moreover, the experimental result[23] that a rapid regeneration (>0.15 s^{-1}) from reduced Cu(I) to the resting Cu(II) state, in the absence of a substrate, was observed by EPR can be also well explained by the *in situ* formation of H_2O_2 by LPMOs. Additionally, the addition of superoxide dismutase was shown to have little effect on H_2O_2 production,[72] which also refutes the dissociation of superoxide species. Therefore, the superoxide dissociation mechanism was not considered further. In principle, the formation of Cu(II)-hydroperoxide from Cu(II)-superoxide may involve either

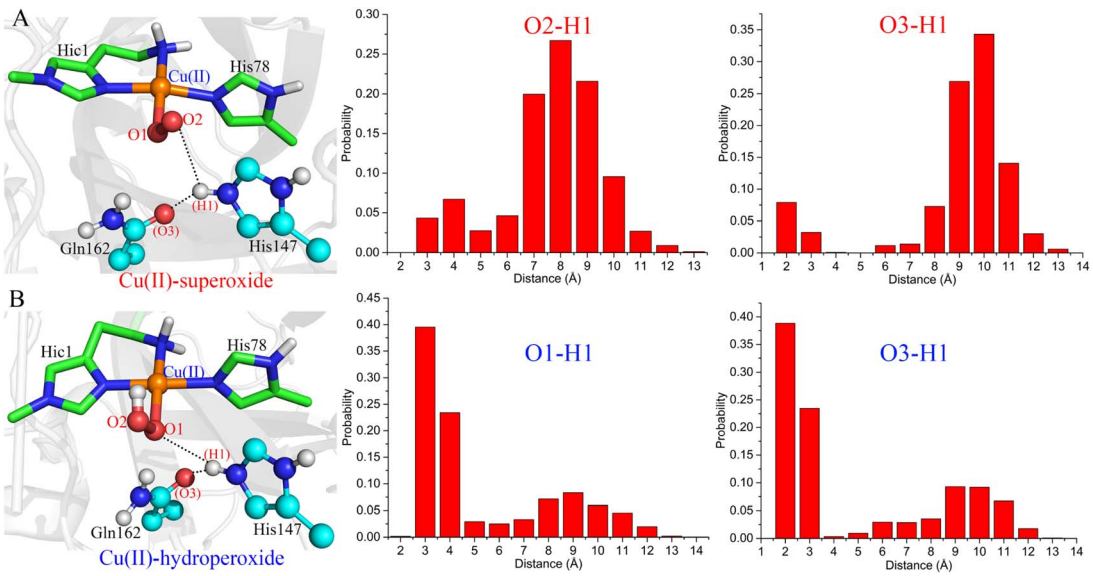

Fig. 3 No direct H-bond forms between His147 and copper-oxide species in (A) Cu(II)-superoxide and (B) Cu(II)-hydroperoxide systems. The structures illustrating the labels of key atoms are shown in the left panel. The statistics of the distance between the origin and destination of the proton transfer reaction in these two systems, the distance between the distal O2 atom and H1 atom in the Cu(II)-superoxide system (O2–H1) and the distance between the proximal O1 atom and H1 atom in the Cu(II)-hydroperoxide system (O1–H1) are shown in the middle panel. Statistics of the distance between the O3 atom of the Gln162 side chain and H1 atom are shown in the right panel, showing the H-bond formed between His147 and the carbonyl group of the Gln162 side chain.

a hydrogen atom transfer or a stepwise PT and ET. In the presence of both the proton supplier (doubly protonated His147) and electron donor (reduced CYT protein), whether protonation of the Cu(II)-superoxide species is coupled with one ET is investigated using QM/MM MD and metadynamics simulations.

Starting with a conformation in which the doubly-protonated His147 forms an H-bond with the side chain of Gln162, the QM/MM MD simulations confirm the stability of this H-bond, with the H1···O3 distance below 2 Å (Fig. S11†). Consistent with the results of classical MD simulations, no direct H-bond between Cu(II)-superoxide and His147 is observed. The distance between H1 and O2 increases from 3.5 Å to 4.5 Å during QM/MM MD simulations (Fig. S11†). The distance between the proximal O1 atom and the copper ion fluctuates around 2.0 Å (Fig. S12†), while the distance between the two oxygen atoms oscillates around 1.3 Å (Fig. S12†). The calculated spin density of the copper ion and the dioxygen moiety is *ca.* 0.65 and 1.15 (Fig. S13†), respectively, further confirming the starting species as Cu(II)-superoxide.[59]

A metadynamics simulation using the distance between the O2 and H1 atoms as the collective variable (CV) shows that the PT reaction is coupled with ET from CYT-Fe(II) to the dioxygen moiety of Cu(II)-superoxide, leading directly to the formation of the Cu(II)-hydroperoxide species. The free energy landscape reconstructed from the metadynamics simulation shows two free energy minima and one metastable intermediate (Fig. 4). In the initial state, RC1 species, the CV fluctuates around 3.5 Å. A metastable intermediate (IC1) forms when the CV decreases to approximately 2.4 Å due to the formation of a weak H-bond between the distal O2 atom and residue His147. As the CV further decreases to 1.0 Å at around 1000 fs during the metadynamics simulation (Fig. 4B), the PT occurs, triggering ET from CYT-Fe(II) to the dioxygen moiety and resulting in the formation of the Cu(II)-hydroperoxide intermediate (PC1 species in Fig. 4). The occurrence of electron transfer is supported by the increase in the spin density of iron from 0.00 to 1.05 and the decrease in the total spin densities of the two oxygen atoms from *ca.* 1.15 to 0.15 (Fig. 4C). After such PCET reaction, the distance between the O1 and O2 atoms increases from 1.3 Å to approximately 1.5 Å (Fig. 4B), consistent with the conversion from a superoxide to peroxide species. The free energy barrier of this PCET process is estimated to be 10.8 kcal mol^{-1} with metadynamics simulations, which is quite low. However, we

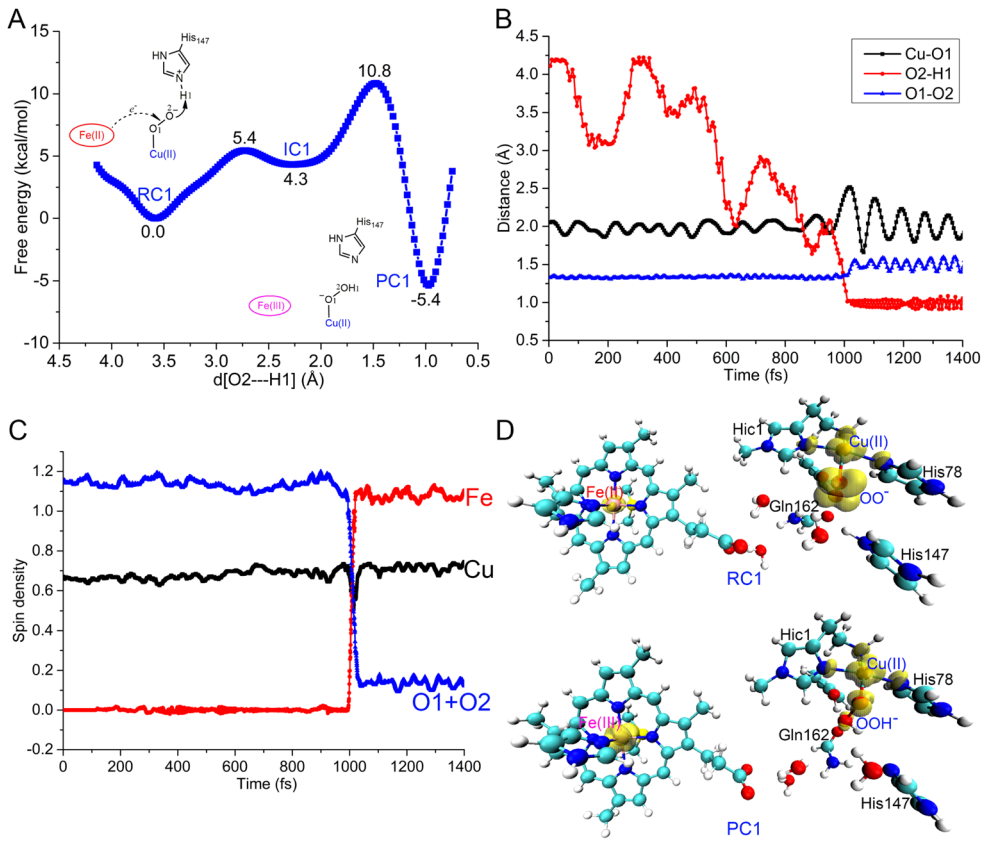

Fig. 4 The PT process from doubly-protonated His147 to Cu(II)-superoxide is coupled with an ET. (A) Free energy profile (kcal mol^{-1}) of the PCET process involved in the formation of Cu(II)-hydroperoxide from Cu(II)-superoxide, reconstructed from QM(B3LYP)/MM-based metadynamics simulations. The collective variable (CV) is the distance between the distal O2 atom and H1 atom of His147. Legend: RC = reactant complex, IC = intermediate complex, and PC = product complex. (B) Time evolution of key distances along the simulation trajectory. (C) Time evolution of the spin density of key atoms or moiety along the simulation trajectory. (D) Representative snapshots of the QM region along the reaction pathway. Spin-up isodensity surfaces are plotted in yellow.

should note that the estimated adiabatic barrier obtained from metadynamics simulations may not be entirely physical due to the involvement of long-range ET between CYT and LPMO.[59] For this reason, we further analyse the corresponding ET rate using Marcus theory below.[89]

3.3. Protonation of Cu(II)-hydroperoxide species occurs *via* the proximal oxygen

Starting from the conformation shown in Fig. 3B, where a strong H-bond forms between His147 and Gln162, proton transfer from doubly protonated His147 to the proximal oxygen O1 atom occurs spontaneously during QM/MM MD simulation (Fig. S14†), indicating the feasibility of this PT reaction. Prior to the reaction, the proton is located on the residue His147, and the iron remains in its reduced form (RC2 in Fig. 5). Unlike the case of Cu(II)-superoxide, this PT process is not found to be coupled with ET. The spin density on iron remains at 0.00 after the PT process (Fig. S15†), indicating the absence of ET. Metadynamics simulations further support that the facile PT from His147 to Cu(II)-hydroperoxide is not coupled with ET. Fig. 5A shows the free energy landscape of this pure PT reaction from Cu(II)-hydroperoxide (RC2) to Cu(II)–H_2O_2 (PC2) reconstructed from the metadynamics simulation. The small free energy barrier of 4.6 kcal mol^{-1} confirms the feasibility of this reaction. Scrutiny of the metadynamics trajectory clearly shows that the PT had occurred without ET. The proton transfers to the acceptor in the time window 150 fs to 350 fs (Fig. S16†), yet the iron atom remains in its reduced state (Fig. S17†). Fig. 5B shows representative structures along with spin density maps of the RC2 and PC2 species, confirming the formation of the Cu(II)–H_2O_2 complex (PC2 in Fig. 5). Subsequently, the newly formed hydrogen peroxide, located at the equatorial position, may be displaced by a water molecule and escape from the active site (Fig. S18†). This mechanism is consistent with the elongation of the Cu···O1 distance after the formation of H_2O_2 (Fig. S14†) and the experimental proposal that substrate-free LPMOs can provide H_2O_2 for substrate-bound LPMOs.[13,25,90] The results obtained here, as well as previous studies,[38,40,91] exclude path d in Scheme 1, previously suggested by Hedegård and Ryde,[39] in which the proton transfers to the distal rather than the proximal oxygen atom.

3.4. PT *vs.* PCET

Next, we seek to understand why the first PT of the reaction mechanism is coupled to an ET yet the second not. When no electron was supplied (*i.e.*, the electron donor is excluded from the QM region), the QM/MM scanning calculations demonstrate that the energy steadily increases as the distance between H1 and O2 atoms (reactive coordinate) decreases (a pure PT process, red line in Fig. 6). The energy increases to 25.9 kcal mol^{-1} when the reactive coordinate reaches 1.02 Å. In contrast, when the electron donor of the reduced CYT was included in the QM region, the energy profile exhibits a sudden decrease when the reactive coordinate decreases to approximately 1.20 Å, indicating an ET from CYT to LPMO and thus a typical PCET process (blue line in Fig. 6). When the reactive coordinate equals 1.00 Å, the scanning energy has decreased to −9.3 kcal mol^{-1}. Therefore, the QM/MM scanning calculations provided further confirmation that the first PT must be coupled with an ET. Additionally, it became evident that without ET, the product $[Cu\text{-}OOH]^{2+}$ formed after the pure PT is an unstable species. This instability is the fundamental reason for the occurrence of PCET. These findings are generally consistent with a very recent QM/MM study by Hagemann *et al.* using a big QM region (up to 900 atoms)[40] and shed light on the importance of ET in stabilizing the intermediate species during the PCET process. Our QM-scanning calculations (details can be found in the ESI Methods of ESI†) showed that the electron affinity increases during the two PT processes (Fig. 7). In the first PT (formation of Cu(II)-hydroperoxide from Cu(II)-superoxide), the electron

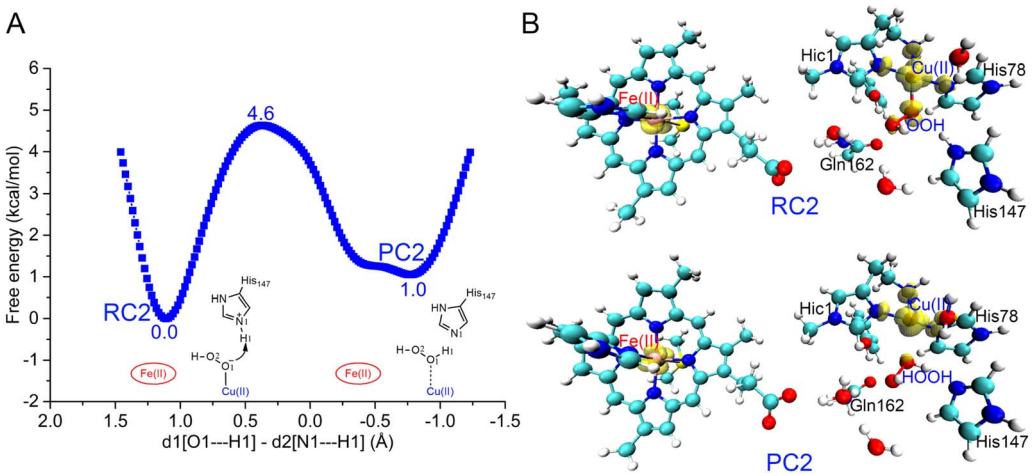

Fig. 5 The PT process from doubly-protonated His147 to Cu(II)-hydroperoxide is not coupled with an ET when reduced CYT is used as the reductant. (A) Free energy profile (kcal mol^{-1}) of the PT process involved in the formation of LPMO-Cu(II) and H_2O_2 from Cu(II)-hydroperoxide, reconstructed from QM(B3LYP)/MM-based metadynamics simulations. The CV is the difference distance between the proximal O1 atom and H1 atom of His147 and between the N1 atom and H1 atom. Legend: RC = reactant complex, PC = product complex. (B) Representative snapshots of the QM region along the reaction pathway. Spin-up isodensity surfaces are plotted in yellow.

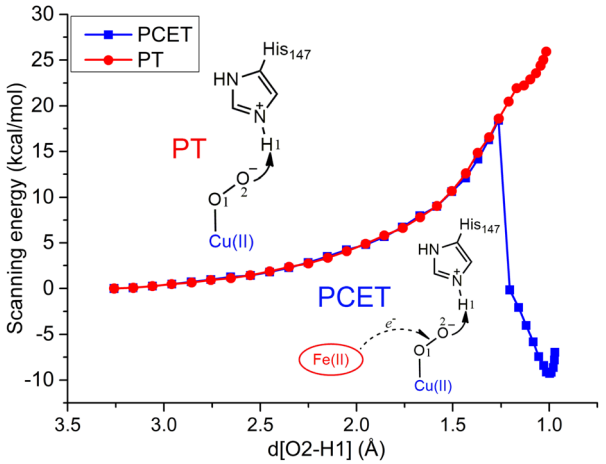

Fig. 6 QM(UB3LYP)/MM scanning energies (kcal mol^{-1}) of the first PT process from His147 to Cu(II)-superoxide with (blue line) or without (red line) the reductant (reduced CYT-Fe(II)) in the QM region. The reactive coordinate used here is the distance between the distal O2 atom and H1 atom of His147. When the reductant is included in the QM region, the PT can induce an ET, leading to a PCET process (blue line), which is much favored over the pure PT process (red line).

affinity increases by 22.4 kcal mol^{-1}, from 76.7 kcal mol^{-1} to 99.1 kcal mol^{-1} (blue line in Fig. 7) as the reaction coordinate (the distance between the distal oxygen O2 and the proton H1, labelled as d1 in Fig. 7) decreases from its initial optimized value of 1.75 Å to 1.00 Å. Similarly, in the second PT from Cu(II)–OOH^- to Cu(II)–H_2O_2, the electron affinity increases by 12.6 kcal mol^{-1} from 75.0 kcal mol^{-1} to 87.6 kcal mol^{-1} as the reaction coordinate (d2, the distance between O1 and H1, inset of Fig. 7) decreases from 1.52 Å to 1.02 Å (red line in Fig. 7). Hence, the ability of the first PT to drive ET from the Cu-superoxide system

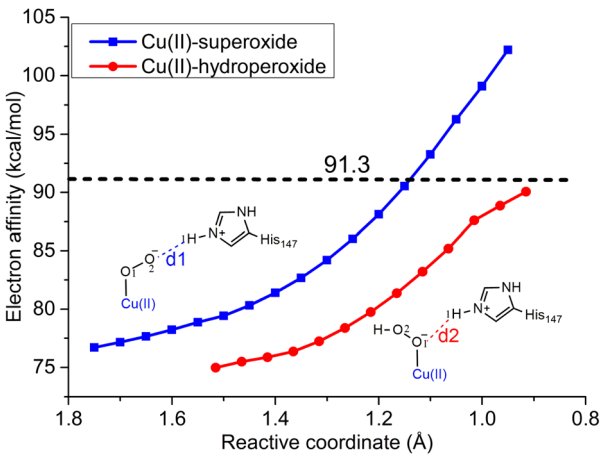

Fig. 7 The change of electron affinity during the first (blue line) and second PT (red line) processes. For the first PT in the Cu(II)-superoxide system, the reactive coordinate is the distance between the distal O2 atom and the H1 atom (d1). For the second PT in the Cu(II)-hydroperoxide system, the reactive coordinate is the distance between the proximal O1 atom and the H1 atom (d2). The ionization energy of CYT-Fe(II) is calculated to be 91.3 kcal mol^{-1}, which is shown by a black dashed line.

is much stronger than that of the second PT from the Cu-hydroperoxide system. When the distance between the proton and its acceptor is approximately 1.0 Å, the electron affinity of the Cu-superoxide system is 11.5 kcal mol^{-1} higher than that of the Cu-hydroperoxide system. It is worth noting that the ionization energy of heme-Fe(II), calculated to be 91.3 kcal mol^{-1} at the same level of theory, is lower than the electron affinity of the Cu(II)-superoxide species yet higher than that of the Cu(II)-hydroperoxide species when the reaction coordinate is approximately 1.0 Å (refer to Fig. 7). Consequently, only the PT to Cu(II)-superoxide can induce long-range ET from heme-Fe(II), while the PT to Cu(II)-hydroperoxide does not.

The above discussion provides an explanation of why the first PT to Cu(II)-superoxide is coupled with an ET, while the second PT to Cu(II)-hydroperoxide species is a pure PT process when CYT is used as the reducing agent. We suggest that the coupling of the PT process with ET in the second PT depends on the properties of the reducing agent. For a strong reductant, with an ionization energy lower than 87.6 kcal mol^{-1}, it may directly reduce Cu(II) to Cu(I),[38] whereas a weak reductant, *i.e.*, CDH investigated herein, cannot do it.

3.5. Estimation of the PCET rate

As noted in our previous study,[59,92] the QM/MM MD simulations may overestimate the rate of a long-range electron transfer reaction. Thus, we estimate the rate of the long-range ET (k_{ET}) involved in the conversion process from Cu(II)-superoxide to Cu(II)-hydroperoxide with Marcus theory, eqn (1).[89,93–95]

$$k_{ET} = \frac{2\pi}{\hbar}|H_{DA}|^2 \frac{1}{\sqrt{4\pi\lambda k_B T}} \exp\left(-\frac{(\lambda + \Delta G)^2}{4\lambda k_B T}\right) \quad (1)$$

k_{ET} is influenced by four key parameters: the driving force (ΔG), reorganization energy (λ), temperature (T) and the electronic coupling between the donor and acceptor (H_{DA}). k_B is the Boltzmann constant, and $\hbar$ is the reduced Planck's constant. λ accounts for the changes in the molecular structure and surrounding environment during the ET process, which can be further divided into inner-sphere reorganization energy (λ_i) and outer-sphere reorganization energy (λ_o). λ_i reflects changes in the geometry of the first-shell ligands around the donor and acceptor, while λ_o accounts for changes in the solvent and protein environment. A smaller reorganization corresponds to a more efficient ET.

In our previous study, the value of the electronic coupling between CYT and LPMO was obtained with a value of 0.47 meV.[59] Using the experimentally determined ET rate of 20.6 s^{-1} and the typical experimental driving force of −150 meV for the ET from CYT-Fe(II) to LPMO-Cu(II) (step a in Scheme 1),[1,41] we got the value of the total reorganization energy of 2.23 eV based on eqn (1).[59] Furthermore, the total inner-sphere reorganization energy for the initial priming ET process was estimated to be 1.07 eV, and thus the outer-sphere energy for the CYT/LPMO system can be derived to be 2.23 eV − 1.07 eV = 1.16 eV.[59] Herein, for the PCET process from Cu(II)-superoxide to Cu(II)-hydroperoxide (step c in Scheme 1), the value of ΔG can be obtained with the above metadynamics simulations,

assumed to be −5.4 kcal mol^{-1} (−0.23 eV, refer to Fig. 4A). Consistent with our previous work,[59] the electronic coupling H_{DA} and the outer-sphere reorganization energy λ_o can be estimated as 0.47 meV and 1.16 eV, respectively. For the inner-sphere reorganization energy λ_i, we re-estimated it due to the change of the inner-sphere geometry, especially for the LPMO part (refer to Fig. S19†). For the CYT and LPMO parts, λ_i was estimated to be 0.05 eV and 1.16 eV, respectively (see the calculation details in the ESI†). With these values, the k_{ET} of the PCET process was estimated to be 20.4 s^{-1} with eqn (1) at 300 K, which is comparable to the ET rate of 20.6 s^{-1} in the initial reduction step (step a in Scheme 1). It is worth noting that the estimation of the λ_i for the LPMO part was based on a geometry in which a direct H-bond forms between the proton donor (H1) and acceptor (O2) (refer to Fig. S19†). However, our above MD simulations indicated that there is no direct H-bond formed between the proton donor and acceptor (refer to Fig. 3A). Thus, the inner-sphere reorganization energy was underestimated by the current calculations, leading to an overestimation of the rate of the PCET reaction from Cu(II)-superoxide to Cu(II)-hydroperoxide. Therefore, our above analysis suggested that the rate of the PCET reaction from Cu(II)-superoxide to Cu(II)-hydroperoxide is slower than the rate of the first priming ET reaction during the reduction of LPMO-Cu(II). This finding is consistent with a significant amount of experimental evidence indicating that the activity of LPMOs is limited by the rate of H_2O_2 formation when O_2 is used as the oxygen source.[13,37,53–57]

3.6. Implication of the catalytic mechanism of LPMOs

As alluded to above, both ascorbate and CDH(CYT) can act as efficient reducing agents to supply electrons for LPMOs. However, there is a substantial difference between them. Ascorbic acid ($AscH^-$) is a relatively poor electron donor yet a good hydrogen atom (an electron and a proton) supplier.[96,97] In contrast, the CYT protein possesses a lower redox potential (*ca.* 0.099–0.163 V and *ca.* 0.35 V for CYT and ascorbate, respectively) yet no active hydrogen atom.[98,99] Consequently, distinct O_2 activation mechanisms have been revealed for these two reductants, summarized in Fig. 8. In the CDH-dependent pathway, the formation of Cu(II)-hydroperoxide from Cu(II)-superoxide proceeds through a PCET process. In this pathway, the electron is supplied by the reduced CYT, while a potential proton supplier, doubly protonated His147, provides the necessary proton. The electron and proton are transferred simultaneously, facilitating the conversion. On the other hand, in the ascorbate-dependent pathway, both the proton and the electron are supplied by an active hydrogen atom from ascorbic acid, resulting in a hydrogen atom transfer (HAT) process.[38] For the subsequent formation of H_2O_2 from Cu(II)-hydroperoxide, the protonation of the proximal O1 atom cannot induce ET from CYT. Therefore, a pure PT process takes place in the CDH-dependent pathway, leading to the formation of LPMO-Cu(II) and the restoration of the resting state. In contrast, the ascorbate-dependent pathway involves a facile HAT process, resulting in the production of the reduced copper site.[38] Overall,

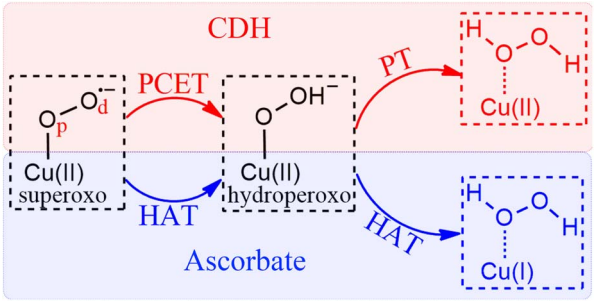

Fig. 8 Comparison between the CDH-dependent O_2 activation mechanism (upper part) and the ascorbate-dependent one (lower part).

the specific O_2 activation mechanism of LPMO is highly dependent on the properties of the reducing agent employed.

Based on the O_2 activation mechanism revealed herein, we further conjecture a catalytic mechanism of LPMO in the presence of CDH and the polysaccharide substrate (Scheme 2). It is generally accepted that the reduction of LPMO occurs before its binding to the polysaccharide substrate,[9] due to the findings that the binding affinity to the polysaccharide substrate is enhanced by the reduction of LPMO[51,100] and when it is bound to the substrate it is inaccessible to the reducing agent.[50,51,59,101,102] Therefore, the binding affinity to the reducing agent (CDH) is expected to be slightly higher than that to the polysaccharide substrate. We note that it has been determined experimentally that the substrate binding affinity increases by only about 1 kcal mol^{-1} due to LPMO reduction.[51] Therefore, it is reasonable to assume that CDH may competitively bind to LPMO even after LPMO reduction. As illustrated in Scheme 2, some reduced LPMO molecules may bind to the substrate and some others may bind to the reducing agent. Such competitive binding picture of the substrate and CDH to LPMO-Cu(I) can rationalize both the generation of H_2O_2 and the substrate oxidation. For LPMO-Cu(I) bound to CDH, it can act as an oxidase to generate H_2O_2. While for LPMO-Cu(I) bound to the substrate, it can employ the H_2O_2 generated from the LPMO/

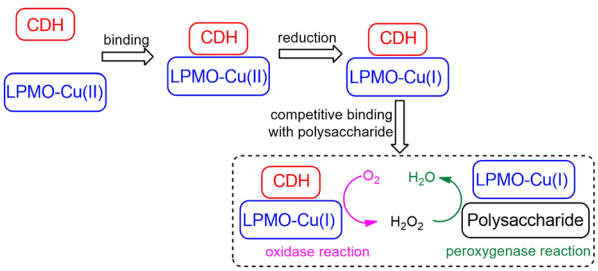

Scheme 2 Proposed catalytic mechanism of LPMO in the presence of CDH and the polysaccharide substrate. Oxidized LPMOs prefer to bind with the reducing agent CDH, yet reduced LPMOs competitively bind with CDH and the polysaccharide substrate. LPMOs bound with CDH can use dioxygen to generate hydrogen peroxide, which can diffuse to the solvent and be used by substrate-bound LPMOs to perform substrate oxidation reactions.

CDH system to perform substrate oxidation reactions *via* the H_2O_2-dependent pathway.[13,19,25,90]

Of note, different LPMOs have been observed to possess divergent oxidase activities,[35,55,103,104] likely due to their different structures and redox potentials.[103] For instance, LPMOs from the AA9 and AA11 families can efficiently produce H_2O_2 through their intrinsic oxidase activities, while LPMOs from the AA10 family largely rely on H_2O_2 generated from the auto-oxidation of reductants.[55,104] Additionally, the proton donors can vary across different LPMOs. In the AA9 family, a doubly-protonated histidine (His) residue has been suggested as the proton donor, while in the AA10 family, a neutral glutamic acid (Glu) residue has been proposed.[20] Therefore, the exact O_2 activation mechanism may vary in different LPMOs families, especially for the second PT reaction that can occur with or without an electron input.

4 Conclusions

In summary, we employ a combination of QM/MM metadynamics simulations, MD simulations, QM calculations, and static QM/MM calculations to investigate the mechanism of dioxygen activation by LPMOs in the presence of the enzymatic reductant CDH. Our study yields the following key findings: (i) dioxygen activation proceeds through a H_2O_2 formation pathway, involving first the formation of Cu(II)-superoxide (Cu(II)-$OO^{\bullet-}$) and, subsequently, Cu(II)-hydroperoxide (Cu(II)-OOH^-). (ii) The conversion from superoxide to hydroperoxide is a PCET process, where the electron is donated by CDH and the proton is donated by the doubly-protonated His147 residue. This step is identified as the rate-limiting step in the overall O_2 activation process. (iii) The transformation from hydroperoxide to H_2O_2 occurs through a pure PT process. Mechanistically, we show that the protonation of the distal O atom of Cu(II)-superoxide, *en route* to the hydroperoxide species, is coupled with an electron input. This coupling can take place through either a PCET or hydrogen atom transfer (HAT) mechanism, depending on the identities of the electron and proton donors. Conversely, the protonation of the proximal oxygen atom of Cu(II)-hydroperoxide, *en route* to H_2O_2, may occur with or without an electron input, depending on the properties of the reductant. In the case of ascorbic acid, which is a poor electron donor yet an efficient H atom donor, two HAT processes are involved during the *in situ* formation of H_2O_2. Therefore, the O_2 activation mechanism of LPMOs is highly dependent on the properties of the reductant. Based on our simulations and previous findings, we propose a catalytic mechanism of LPMO in the presence of CDH and the polysaccharide substrate, which involves the competitive binding of the substrate and CDH to the reduced LPMOs. While the CDH-bound LPMOs can activate dioxygen to generate H_2O_2, the substrate-bound LPMOs can employ the H_2O_2 generated from the LPMO/CDH system to perform the peroxygenase reactions of the polysaccharide substrate. These mechanistic insights contribute to our understanding of the chemistry of LPMOs in their natural environment.

Data availability

The data supporting this article have been included as part of the ESI.†

Author contributions

Z. W.: conceptualization, investigation, formal analysis, methodology, resources, writing, supervision, funding acquisition, review & editing; X. F.: investigation, formal analysis, review & editing; W. D.: formal analysis, review & editing; Y. W.: investigation, formal analysis, methodology, review & editing; C. R.: funding acquisition, supervision, methodology, review & editing; B. W.: funding acquisition, resources, conceptualization, supervision, review & editing.

Conflicts of interest

There are no conflicts to declare.

Acknowledgements

This work was supported by the National Natural Science Foundation of China (no. 22203007 to Z. W., no. 22073077 and 22122305 to B. W.), the Start-up Funding from Beijing Normal University (no. 310432104 to Z. W.), the Spanish Ministry of Science, Innovation and Universities (MICINN/AEI/FEDER, UE, PID2020-118893GB-100), the Spanish Structures of Excellence María de Maeztu (CEX2021-001202-M) and the Agency for Management of University and Research Grants of Catalonia (AGAUR, 2021-SGR-00680). Dr Z. Wang is supported by the Interdisciplinary Intelligence SuperComputer Center of Beijing Normal University Zhuhai.

Notes and references

1 K. K. Meier, S. M. Jones, T. Kaper, H. Hansson, M. J. Koetsier, S. Karkehabadi, E. I. Solomon, M. Sandgren and B. Kelemen, Oxygen Activation by Cu LPMOs in Recalcitrant Carbohydrate Polysaccharide Conversion to Monomer Sugars, *Chem. Rev.*, 2018, **118**, 2593–2635.
2 K. S. Johansen, Discovery and industrial applications of lytic polysaccharide mono-oxygenases, *Biochem. Soc. Trans.*, 2016, **44**, 143–149.
3 X. Cai, J. Hua, Z. M. Lin, C. Y. Sun, C. H. Hu, X. J. Zhang, J. D. Shen, H. Y. Zhou, H. Y. Wang, K. Q. Chen, D. S. Chen, X. P. Cheng, M. Li, Z. Q. Liu and Y. G. Zheng, Enhanced Enzymatic Hydrolysis of High-Solids Content Corncobs by a Lytic Polysaccharide Monooxygenase from Podospora anserina S Mat$^+$ for Valuable Monosaccharides, *ACS Sustainable Chem. Eng.*, 2023, **11**, 9858–9867.
4 X. Qin, K. Yang, X. L. Wang, T. Tu, Y. Wang, J. Zhang, X. Y. Su, B. Yao, H. Q. Huang and H. Y. Luo, Insights into the H_2O_2-Driven Lytic Polysaccharide Monooxygenase Activity on Efficient Cellulose Degradation in the White

Rot Fungus Irpex lacteus, *J. Agric. Food Chem.*, 2023, **71**, 8104–8111.

5 G. Vaaje-Kolstad, B. Westereng, S. J. Horn, Z. L. Liu, H. Zhai, M. Sorlie and V. G. H. Eijsink, An Oxidative Enzyme Boosting the Enzymatic Conversion of Recalcitrant Polysaccharides, *Science*, 2010, **330**, 219–222.

6 P. Chylenski, B. Bissaro, M. Sorlie, Å. K. Rohr, A. Várnai, S. J. Horn and V. G. H. Eijsink, Lytic Polysaccharide Monooxygenases in Enzymatic Processing of Lignocellulosic Biomass, *ACS Catal.*, 2019, **9**, 4970–4991.

7 X. Guo, Y. J. An, F. F. Liu, F. P. Lu and B. Wang, Lytic polysaccharide monooxygenase-A new driving force for lignocellulosic biomass degradation, *Bioresour. Technol.*, 2022, **362**, 127803.

8 B. Bissaro, A. Várnai, A. K. Rohr and V. G. H. Eijsink, Oxidoreductases and Reactive Oxygen Species in Conversion of Lignocellulosic Biomass, *Microbiol. Mol. Biol. Rev.*, 2018, **82**, e00029.

9 A. Munzone, V. G. H. Eijsink, J. G. Berrin and B. Bissaro, Expanding the catalytic landscape of metalloenzymes with lytic polysaccharide monooxygenases, *Nat. Rev. Chem*, 2024, **8**, 106–119.

10 L. Ciano, G. J. Davies, W. B. Tolman and P. H. Walton, Bracing copper for the catalytic oxidation of C-H bonds, *Nat. Catal.*, 2018, **1**, 571–577.

11 R. J. Quinlan, M. D. Sweeney, L. Lo Leggio, H. Otten, J. C. N. Poulsen, K. S. Johansen, K. B. R. M. Krogh, C. I. Jorgensen, M. Tovborg, A. Anthonsen, T. Tryfona, C. P. Walter, P. Dupree, F. Xu, G. J. Davies and P. H. Walton, Insights into the oxidative degradation of cellulose by a copper metalloenzyme that exploits biomass components, *Proc. Natl. Acad. Sci., India*, 2011, **108**, 15079–15084.

12 G. Vaaje-Kolstad, Z. Forsberg, J. S. M. Loose, B. Bissaro and V. G. H. Eijsink, Structural diversity of lytic polysaccharide monooxygenases, *Curr. Opin. Struct. Biol.*, 2017, **44**, 67–76.

13 B. Bissaro, Å. K. Rohr, G. Müller, P. Chylenski, M. Skaugen, Z. Forsberg, S. J. Horn, G. Vaaje-Kolstad and V. G. H. Eijsink, Oxidative cleavage of polysaccharides by monocopper enzymes depends on H2O2, *Nat. Chem. Biol.*, 2017, **13**, 1123–1128.

14 M. M. Hagemann and E. D. Hedegard, Molecular Mechanism of Substrate Oxidation in Lytic Polysaccharide Monooxygenases: Insight from Theoretical Investigations, *Chem.–Eur. J.*, 2023, **29**, e202202379.

15 B. Bissaro, B. Streit, I. Isaksen, V. G. H. Eijsink, G. T. Beckham, J. L. DuBois and Å. K. Rohr, Molecular mechanism of the chitinolytic peroxygenase reaction, *Proc. Natl. Acad. Sci., India*, 2020, **117**, 1504–1513.

16 S. Kim, J. Ståhlberg, M. Sandgren, R. S. Paton and G. T. Beckham, Quantum mechanical calculations suggest that lytic polysaccharide monooxygenases use a copper-oxyl, oxygen-rebound mechanism, *Proc. Natl. Acad. Sci., India*, 2014, **111**, 149–154.

17 E. D. Hedegård and U. Ryde, Targeting the reactive intermediate in polysaccharide monooxygenases, *J. Biol. Inorg. Chem.*, 2017, **22**, 1029–1037.

18 L. Bertini, R. Breglia, M. Lambrughi, P. Fantucci, L. De Gioia, M. Borsari, M. Sola, C. A. Bortolotti and M. Bruschi, Catalytic Mechanism of Fungal Lytic Polysaccharide Monooxygenases Investigated by First-Principles Calculations, *Inorg. Chem.*, 2018, **57**, 86–97.

19 B. J. Wang, E. M. Johnston, P. F. Li, S. Shaik, G. J. Davies, P. H. Walton and C. Rovira, QM/MM Studies into the H2O2-Dependent Activity of Lytic Polysaccharide Monooxygenases: Evidence for the Formation of a Caged Hydroxyl Radical Intermediate, *ACS Catal.*, 2018, **8**, 1346–1351.

20 O. Caldararu, E. Oksanen, U. Ryde and E. D. Hedegård, Mechanism of hydrogen peroxide formation by lytic polysaccharide monooxygenase, *Chem. Sci.*, 2019, **10**, 576–586.

21 H. Lim, M. T. Brueggemeyer, W. J. Transue, K. K. Meier, S. M. Jones, T. Kroll, D. Sokaras, B. Kelemen, B. Hedman, K. O. Hodgson and E. I. Solomon, Kβ X-ray Emission Spectroscopy of Cu(I)-Lytic Polysaccharide Monooxygenase: Direct Observation of the Frontier Molecular Orbital for H_2O_2 Activation, *J. Am. Chem. Soc.*, 2023, **145**, 16015–16025.

22 W. T. Beeson, C. M. Phillips, J. H. D. Cate and M. A. Marletta, Oxidative Cleavage of Cellulose by Fungal Copper-Dependent Polysaccharide Monooxygenases, *J. Am. Chem. Soc.*, 2012, **134**, 890–892.

23 C. H. Kjaergaard, M. F. Qayyum, S. D. Wong, F. Xu, G. R. Hemsworth, D. J. Walton, N. A. Young, G. J. Davies, P. H. Walton, K. S. Johansen, K. O. Hodgson, B. Hedman and E. I. Solomon, Spectroscopic and computational insight into the activation of O_2 by the mononuclear Cu center in polysaccharide monooxygenases, *Proc. Natl. Acad. Sci., India*, 2014, **111**, 8797–8802.

24 G. Courtade, L. Ciano, A. Paradisi, P. J. Lindley, Z. Forsberg, M. Sorlie, R. Wimmer, G. J. Davies, V. G. H. Eijsink, P. H. Walton and F. L. Aachmann, Mechanistic basis of substrate-O_2 coupling within a chitin-active lytic polysaccharide monooxygenase: An integrated NMR/EPR study, *Proc. Natl. Acad. Sci., India*, 2020, **117**, 19178–19189.

25 J. A. Hangasky, A. T. Iavarone and M. A. Marletta, Reactivity of O_2 *versus* H_2O_2 with polysaccharide monooxygenases, *Proc. Natl. Acad. Sci., India*, 2018, **115**, 4915–4920.

26 S. Kuusk, B. Bissaro, P. Kuusk, Z. Forsberg, V. G. H. Eijsink, M. Sorlie and P. Väljamäe, Kinetics of H2O2-driven degradation of chitin by a bacterial lytic polysaccharide monooxygenase, *J. Biol. Chem.*, 2018, **293**, 523–531.

27 R. Kont, B. Bissaro, V. G. H. Eijsink and P. Väljamäe, Kinetic insights into the peroxygenase activity of cellulose-active lytic polysaccharide monooxygenases (LPMOs), *Nat. Commun.*, 2020, **11**, 5786.

28 T. M. Hedison, E. Breslmayr, M. Shanmugam, K. Karnpakdee, D. J. Heyes, A. P. Green, R. Ludwig, N. S. Scrutton and D. Kracher, Insights into the H_2O_2-driven catalytic mechanism of fungal lytic polysaccharide monooxygenases, *FEBS J.*, 2021, **288**, 4115–4128.

29 S. Brander, R. Tokin, J. O. Ipsen, P. E. Jensen, C. Hernández-Rollán, M. H. H. Norholm, L. Lo Leggio, P. Dupree and

K. S. Johansen, Scission of Glucosidic Bonds by a *Lentinus similis* Lytic Polysaccharide Monooxygenases Is Strictly Dependent on H_2O_2 while the Oxidation of Saccharide Products Depends on O_2, *ACS Catal.*, 2021, **11**, 13848–13859.

30 D. Kracher, Z. Forsberg, B. Bissaro, S. Gangl, M. Preims, C. Sygmund, V. G. H. Eijsink and R. Ludwig, Polysaccharide oxidation by lytic polysaccharide monooxygenase is enhanced by engineered cellobiose dehydrogenase, *FEBS J.*, 2020, **287**, 897–908.

31 W. Gao and H. Yin, Insight into the peroxygenase activity of lytic polysaccharide monooxygenases (LPMO): Recent progress and mechanistic understanding, *Chem. Phys. Rev.*, 2023, **4**, 031310.

32 R. Kittl, D. Kracher, D. Burgstaller, D. Haltrich and R. Ludwig, Production of four Neurospora crassa lytic polysaccharide monooxygenases in Pichia pastoris monitored by a fluorimetric assay, *Biotechnol. Biofuels*, 2012, **5**, 79.

33 K. R. Hall, C. Joseph, I. Ayuso-Fernández, A. Tamhankar, L. Rieder, R. Skaali, O. Golten, F. Neese, Å. K. Rohr, S. A. V. Jannuzzi, S. DeBeer, V. G. H. Eijsink and M. Sorlie, A Conserved Second Sphere Residue Tunes Copper Site Reactivity in Lytic Polysaccharide Monooxygenases, *J. Am. Chem. Soc.*, 2023, **145**, 18888–18903.

34 K. Chorozian, A. Karnaouri, N. Georgaki-Kondyli, A. Karantonis and E. Topakas, Assessing the role of redox partners in *Tth*LPMO9G and its mutants: focus on H_2O_2 production and interaction with cellulose, *Biotechnol. Biofuels*, 2024, **17**, 19.

35 L. Rieder, A. A. Stepnov, M. Sorlie and V. G. H. Eijsink, Fast and Specific Peroxygenase Reactions Catalyzed by Fungal Mono-Copper Enzymes, *Biochemistry*, 2021, **60**, 3633–3643.

36 F. Li, F. Y. Ma, H. L. Zhao, S. Zhang, L. Wang, X. Y. Zhang and H. B. Yu, A Lytic Polysaccharide Monooxygenase from a White-Rot Fungus Drives the Degradation of Lignin by a Versatile Peroxidase, *Appl. Environ. Microbiol.*, 2019, **85**, e02803–e02818.

37 A. A. Stepnov, V. G. H. Eijsink and Z. Forsberg, Enhanced *in situ* H2O2 production explains synergy between an LPMO with a cellulose-binding domain and a single-domain LPMO, *Sci. Rep.*, 2022, **12**, 6129.

38 B. J. Wang, P. H. Walton and C. Rovira, Molecular Mechanisms of Oxygen Activation and Hydrogen Peroxide Formation in Lytic Polysaccharide Monooxygenases, *ACS Catal.*, 2019, **9**, 4958–4969.

39 E. D. Hedegård and U. Ryde, Molecular mechanism of lytic polysaccharide monooxygenases, *Chem. Sci.*, 2018, **9**, 3866–3880.

40 M. M. Hagemann, E. K. Wieduwilt, U. Ryde and E. D. Hedegård, Investigating the Substrate Oxidation Mechanism in Lytic Polysaccharide Monooxygenase: H_2O_2- *versus* O_2-Activation, *Inorg. Chem.*, 2024, **63**, 21929–21940.

41 D. Kracher, S. Scheiblbrandner, A. K. G. Felice, E. Breslmayr, M. Preims, K. Ludwicka, D. Haltrich, V. G. H. Eijsink and R. Ludwig, Extracellular electron transfer systems fuel cellulose oxidative degradation, *Science*, 2016, **352**, 1098–1101.

42 L. Zhang, C. V. F. P. Laurent, L. Schwaiger, L. S. Wang, S. Ma and R. Ludwig, Interdomain Linker of the Bioelecrocatalyst Cellobiose Dehydrogenase Governs the Electron Transfer, *ACS Catal.*, 2023, **13**, 8195–8205.

43 J. S. M. Loose, Z. Forsberg, D. Kracher, S. Scheiblbrandner, R. Ludwig, V. G. H. Eijsink and G. Vaaje-Kolstad, Activation of bacterial lytic polysaccharide monooxygenases with cellobiose dehydrogenase, *Protein Sci.*, 2016, **25**, 2175–2186.

44 G. C. Schröder, W. B. O'Dell, S. P. Webb, P. K. Agarwal and F. Meilleur, Capture of activated dioxygen intermediates at the copper-active site of a lytic polysaccharide monooxygenase, *Chem. Sci.*, 2022, **13**, 13303–13320.

45 G. Müller, P. Chylenski, B. Bissaro, V. G. H. Eijsink and S. J. Horn, The impact of hydrogen peroxide supply on LPMO activity and overall saccharification efficiency of a commercial cellulase cocktail, *Biotechnol. Biofuels*, 2018, **11**, 209.

46 F. Filandr, D. Kavan, D. Kracher, C. V. F. P. Laurent, R. Ludwig, P. Man and P. Halada, Structural Dynamics of Lytic Polysaccharide Monooxygenase during Catalysis, *Biomolecules*, 2020, **10**, 242.

47 A. Kadic, A. Várnai, V. G. H. Eijsink, S. J. Horn and G. Lidén, In situ measurements of oxidation-reduction potential and hydrogen peroxide concentration as tools for revealing LPMO inactivation during enzymatic saccharification of cellulose, *Biotechnol. Biofuels*, 2021, **14**, 46.

48 I. A. Christensen, V. G. H. Eijsink, A. A. Stepnov, G. Courtade and F. L. Aachmann, Following the Fate of Lytic Polysaccharide Monooxygenases under Oxidative Conditions by NMR Spectroscopy, *Biochemistry*, 2023, **62**, 1976–1993.

49 C. M. Phillips, W. T. Beeson, J. H. Cate and M. A. Marletta, Cellobiose Dehydrogenase and a Copper-Dependent Polysaccharide Monooxygenase Potentiate Cellulose Degradation by *Neurospora crassa*, *ACS Chem. Biol.*, 2011, **6**, 1399–1406.

50 T. C. Tan, D. Kracher, R. Gandini, C. Sygmund, R. Kittl, D. Haltrich, B. M. Hällberg, R. Ludwig and C. Divne, Structural basis for cellobiose dehydrogenase action during oxidative cellulose degradation, *Nat. Commun.*, 2015, **6**, 7542.

51 G. Courtade, R. Wimmer, Å. K. Rohr, M. Preims, A. K. G. Felice, M. Dimarogona, G. Vaaje-Kolstad, M. Sorlie, M. Sandgren, R. Ludwig, V. G. H. Eijsink and F. L. Aachmann, Interactions of a fungal lytic polysaccharide monooxygenase with β-glucan substrates and cellobiose dehydrogenase, *Proc. Natl. Acad. Sci., India*, 2016, **113**, 5922–5927.

52 M. Frommhagen, M. J. Koetsier, A. H. Westphal, J. Visser, S. W. A. Hinz, J. P. Vincken, W. J. H. van Berkel, M. A. Kabel and H. Gruppen, Lytic polysaccharide monooxygenases from *Myceliophthora thermophila* C1 differ in substrate preference and reducing agent specificity, *Biotechnol. Biofuels*, 2016, **9**, 186.

53 O. Golten, I. Ayuso-Fernández, K. R. Hall, A. A. Stepnov, M. Sorlie, Å. K. Rohr and V. G. H. Eijsink, Reductants fuel lytic polysaccharide monooxygenase activity in a pH-dependent manner, *FEBS Lett.*, 2023, **597**, 1363–1374.
54 F. Filandr, P. Man, P. Halada, H. H. Chang, R. Ludwig and D. Kracher, The H_2O_2-dependent activity of a fungal lytic polysaccharide monooxygenase investigated with a turbidimetric assay, *Biotechnol. Biofuels*, 2020, **13**, 37.
55 A. A. Stepnov, Z. Forsberg, M. Sorlie, G. S. Nguyen, A. Wentzel, A. K. Rohr and V. G. H. Eijsink, Unraveling the roles of the reductant and free copper ions in LPMO kinetics, *Biotechnol. Biofuels*, 2021, **14**, 28.
56 O. A. Hegnar, D. M. Petrovic, B. Bissaro, G. Alfredsen, A. Várnai and V. G. H. Eijsink, pH-Dependent Relationship between Catalytic Activity and Hydrogen Peroxide Production Shown *via* Characterization of a Lytic Polysaccharide Monooxygenase from *Gloeophyllum trabeum*, *Appl. Environ. Microbiol.*, 2019, **85**, e02612–e02618.
57 A. A. Stepnov, I. A. Christensen, Z. Forsberg, F. L. Aachmann, G. Courtade and V. G. H. Eijsink, The impact of reductants on the catalytic efficiency of a lytic polysaccharide monooxygenase and the special role of dehydroascorbic acid, *FEBS Lett.*, 2022, **596**, 53–70.
58 K. E. H. Frandsen, T. J. Simmons, P. Dupree, J. C. N. Poulsen, G. R. Hemsworth, L. Ciano, E. M. Johnston, M. Tovborg, K. S. Johansen, P. von Freiesleben, L. Marmuse, S. Fort, S. Cottaz, H. Driguez, B. Henrissat, N. Lenfant, F. Tuna, A. Baldansuren, G. J. Davies, L. Lo Leggio and P. H. Walton, The molecular basis of polysaccharide cleavage by lytic polysaccharide monooxygenases, *Nat. Chem. Biol.*, 2016, **12**, 298–303.
59 Z. F. Wang, S. S. Feng, C. Rovira and B. J. Wang, How Oxygen Binding Enhances Long-Range Electron Transfer: Lessons From Reduction of Lytic Polysaccharide Monooxygenases by Cellobiose Dehydrogenase, *Angew. Chem. Int. Ed.*, 2021, **60**, 2385–2392.
60 P. F. Li and K. M. Merz, MCPB.py: A Python Based Metal Center Parameter Builder, *J. Chem. Inf. Model.*, 2016, **56**, 599–604.
61 P. F. Li and K. M. Merz, Metal Ion Modeling Using Classical Mechanics, *Chem. Rev.*, 2017, **117**, 1564–1686.
62 J. A. Maier, C. Martinez, K. Kasavajhala, L. Wickstrom, K. E. Hauser and C. Simmerling, ff14SB: Improving the Accuracy of Protein Side Chain and Backbone Parameters from ff99SB, *J. Chem. Theory Comput.*, 2015, **11**, 3696–3713.
63 J. A. Izaguirre, D. P. Catarello, J. M. Wozniak and R. D. Skeel, Langevin stabilization of molecular dynamics, *J. Chem. Phys.*, 2001, **114**, 2090–2098.
64 H. J. C. Berendsen, J. P. M. Postma, W. F. Vangunsteren, A. Dinola and J. R. Haak, Molecular-Dynamics with Coupling to an External Bath, *J. Chem. Phys.*, 1984, **81**, 3684–3690.
65 V. Krautler, W. F. Van Gunsteren and P. H. Hunenberger, A fast SHAKE: Algorithm to solve distance constraint equations for small molecules in molecular dynamics simulations, *J. Comput. Chem.*, 2001, **22**, 501–508.
66 T. Darden, D. York and L. Pedersen, Particle Mesh Ewald - an N.Log(N) Method for Ewald Sums in Large Systems, *J. Chem. Phys.*, 1993, **98**, 10089–10092.
67 R. Salomon-Ferrer, A. W. Götz, D. Poole, S. Le Grand and R. C. Walker, Routine Microsecond Molecular Dynamics Simulations with AMBER on GPUs. 2. Explicit Solvent Particle Mesh Ewald, *J. Chem. Theory Comput.*, 2013, **9**, 3878–3888.
68 A. W. Götz, M. J. Williamson, D. Xu, D. Poole, S. Le Grand and R. C. Walker, Routine Microsecond Molecular Dynamics Simulations with AMBER on GPUs. 1. Generalized Born, *J. Chem. Theory Comput.*, 2012, **8**, 1542–1555.
69 S. Le Grand, A. W. Götz and R. C. Walker, SPFP: Speed without compromise-A mixed precision model for GPU accelerated molecular dynamics simulations, *Comput. Phys. Commun.*, 2013, **184**, 374–380.
70 J. M. Swails, D. M. York and A. E. Roitberg, Constant pH Replica Exchange Molecular Dynamics in Explicit Solvent Using Discrete Protonation States: Implementation, Testing, and Validation, *J. Chem. Theory Comput.*, 2014, **10**, 1341–1352.
71 W. B. O'Dell, P. K. Agarwal and F. Meilleur, Oxygen Activation at the Active Site of a Fungal Lytic Polysaccharide Monooxygenase, *Angew. Chem. Int. Ed.*, 2017, **56**, 767–770.
72 E. A. Span, D. L. M. Suess, M. C. Deller, R. D. Britt and M. A. Marletta, The Role of the Secondary Coordination Sphere in a Fungal Polysaccharide Monooxygenase, *ACS Chem. Biol.*, 2017, **12**, 1095–1103.
73 T. D. Kuhne, M. Iannuzzi, M. Del Ben, V. V. Rybkin, P. Seewald, F. Stein, T. Laino, R. Z. Khaliullin, O. Schutt, F. Schiffmann, D. Golze, J. Wilhelm, S. Chulkov, M. H. Bani-Hashemian, V. Weber, U. Borstnik, M. Taillefumier, A. S. Jakobovits, A. Lazzaro, H. Pabst, T. Muller, R. Schade, M. Guidon, S. Andermatt, N. Holmberg, G. K. Schenter, A. Hehn, A. Bussy, F. Belleflamme, G. Tabacchi, A. Gloss, M. Lass, I. Bethune, C. J. Mundy, C. Plessl, M. Watkins, J. VandeVondele, M. Krack and J. Hutter, CP2K: An electronic structure and molecular dynamics software package - Quickstep: Efficient and accurate electronic structure calculations, *J. Chem. Phys.*, 2020, **152**, 194103.
74 J. VandeVondele, M. Krack, F. Mohamed, M. Parrinello, T. Chassaing and J. Hutter, QUICKSTEP: Fast and accurate density functional calculations using a mixed Gaussian and plane waves approach, *Comput. Phys. Commun.*, 2005, **167**, 103–128.
75 T. Laino, F. Mohamed, A. Laio and M. Parrinello, An efficient real space multigrid OM/MM electrostatic coupling, *J. Chem. Theory Comput.*, 2005, **1**, 1176–1184.
76 A. Laio, J. VandeVondele and U. Rothlisberger, A Hamiltonian electrostatic coupling scheme for hybrid Car-Parrinello molecular dynamics simulations, *J. Chem. Phys.*, 2002, **116**, 6941–6947.

77 J. VandeVondele and J. Hutter, Gaussian basis sets for accurate calculations on molecular systems in gas and condensed phases, *J. Chem. Phys.*, 2007, **127**, 114105.
78 C. Hartwigsen, S. Goedecker and J. Hutter, Relativistic separable dual-space Gaussian pseudopotentials from H to Rn, *Phys. Rev. B:Condens. Matter Mater. Phys.*, 1998, **58**, 3641–3662.
79 S. Goedecker, M. Teter and J. Hutter, Separable dual-space Gaussian pseudopotentials, *Phys. Rev. B:Condens. Matter Mater. Phys.*, 1996, **54**, 1703–1710.
80 M. Guidon, J. Hutter and J. VandeVondele, Auxiliary Density Matrix Methods for Hartree-Fock Exchange Calculations, *J. Chem. Theory Comput.*, 2010, **6**, 2348–2364.
81 A. Barducci, G. Bussi and M. Parrinello, Well-tempered metadynamics: A smoothly converging and tunable free-energy method, *Phys. Rev. Lett.*, 2008, **100**, 020603.
82 A. Laio and M. Parrinello, Escaping free-energy minima, *Proc. Natl. Acad. Sci., India*, 2002, **99**, 12562–12566.
83 B. Ensing, A. Laio, M. Parrinello and M. L. Klein, A recipe for the computation of the free energy barrier and the lowest free energy path of concerted reactions, *J. Phys. Chem. B*, 2005, **109**, 6676–6687.
84 S. Banerjee, S. J. Muderspach, T. Tandrup, K. E. H. Frandsen, R. K. Singh, J. O. Ipsen, C. Hernández-Rollán, M. H. H. Norholm, M. J. Bjerrum, K. S. Johansen and L. Lo Leggio, Protonation State of an Important Histidine from High Resolution Structures of Lytic Polysaccharide Monooxygenases, *Biomolecules*, 2022, **12**, 194.
85 I. Isaksen, S. Jana, C. M. Payne, B. Bissaro and Å. K. Rohr, The rotamer of the second-sphere histidine in AA9 lytic polysaccharide monooxygenase is pH dependent, *Biophys. J.*, 2024, **123**, 1139–1151.
86 C. M. Payne, B. C. Knott, H. B. Mayes, H. Hansson, M. E. Himmel, M. Sandgren, J. Ståhlberg and G. T. Beckham, Fungal Cellulases, *Chem. Rev.*, 2015, **115**, 1308–1448.
87 W. Purahong, T. Wubet, G. Lentendu, B. Hoppe, K. Jariyavidyanont, T. Arnstadt, K. Baber, P. Otto, H. Kellner, M. Hofrichter, J. Bauhus, W. W. Weisser, D. Krüger, E. D. Schulze, T. Kahl and F. Buscot, Determinants of Deadwood-Inhabiting Fungal Communities in Temperate Forests: Molecular Evidence From a Large Scale Deadwood Decomposition Experiment, *Front. Microbiol.*, 2018, **9**, 2120.
88 C. C. Moser, J. M. Keske, K. Warncke, R. S. Farid and P. L. Dutton, Nature of Biological Electron-Transfer, *Nature*, 1992, **355**, 796–802.
89 R. A. Marcus and N. Sutin, Electron Transfers in Chemistry and Biology, *Biochim. Biophys. Acta*, 1985, **811**, 265–322.
90 H. C. Zhou, Y. B. Zhang, T. Li, H. D. Tan, G. H. Li and H. Yin, Distinct Interaction of Lytic Polysaccharide Monooxygenase with Cellulose Revealed by Computational and Biochemical Studies, *J. Phys. Chem. Lett.*, 2020, **11**, 3987–3992.
91 B. J. Wang, Z. F. Wang, G. J. Davies, P. H. Walton and C. Rovira, Activation of O_2 and H_2O_2 by Lytic Polysaccharide Monooxygenases, *ACS Catal.*, 2020, **10**, 12760–12769.
92 W. H. Fang, S. S. Feng, Z. H. Jiang, W. Z. Liang, P. F. Li and B. J. Wang, Understanding the Key Roles of pH Buffer in Accelerating Lignin Degradation by Lignin Peroxidase, *JACS Au*, 2023, **3**, 536–549.
93 S. Hammes-Schiffer and A. V. Soudackov, Proton-Coupled Electron Transfer in Solution, Proteins, and Electrochemistry, *J. Phys. Chem. B*, 2008, **112**, 14108–14123.
94 M. C. Kessinger, J. Xu, K. Cui, Q. Loague, A. V. Soudackov, S. Hammes-Schiffer and G. J. Meyer, Direct Evidence for a Sequential Electron Transfer-Proton Transfer Mechanism in the PCET Reduction of a Metal Hydroxide Catalyst, *J. Am. Chem. Soc.*, 2024, **146**, 1742–1747.
95 A. Nilsen-Moe, C. R. Reinhardt, P. Huang, H. Agarwala, R. Lopes, M. Lasagna, S. Glover, S. Hammes-Schiffer, C. Tommos and L. Hammarstroem, Switching the proton-coupled electron transfer mechanism for non-canonical tyrosine residues in a *de novo* protein, *Chem. Sci.*, 2024, **15**, 3957–3970.
96 D. Njus and P. M. Kelley, Vitamin-C and Vitamin-E Donate Single Hydrogen-Atoms Invivo, *FEBS Lett.*, 1991, **284**, 147–151.
97 D. Njus, P. M. Kelley, Y. J. Tu and H. B. Schlegel, Ascorbic acid: The chemistry underlying its antioxidant properties, *Free Radical Biol. Med.*, 2020, **159**, 37–43.
98 C. Sygmund, D. Kracher, S. Scheiblbrandner, K. Zahma, A. K. G. Felice, W. Harreither, R. Kittl and R. Ludwig, Characterization of the Two *Neurospora crassa* Cellobiose Dehydrogenases and Their Connection to Oxidative Cellulose Degradation, *Appl. Environ. Microbiol.*, 2012, **78**, 6161–6171.
99 T. Matsui, Y. Kitagawa, M. Okumura and Y. Shigeta, Accurate Standard Hydrogen Electrode Potential and Applications to the Redox Potentials of Vitamin C and NAD/NADH, *J. Phys. Chem. A*, 2015, **119**, 369–376.
100 D. Kracher, M. Andlar, P. G. Furtmüller and R. Ludwig, Active-site copper reduction promotes substrate binding of fungal lytic polysaccharide monooxygenase and reduces stability, *J. Biol. Chem.*, 2018, **293**, 1676–1687.
101 C. V. F. P. Laurent, E. Breslmayr, D. Tunega, R. Ludwig and C. Oostenbrink, Interaction between Cellobiose Dehydrogenase and Lytic Polysaccharide Monooxygenase, *Biochemistry*, 2019, **58**, 1226–1235.
102 B. Bissaro, I. Isaksen, G. Vaaje-Kolstad, V. G. H. Eijsink and Å. K. Rohr, How a Lytic Polysaccharide Monooxygenase Binds Crystalline Chitin, *Biochemistry*, 2018, **57**, 1893–1906.
103 L. Rieder, D. Petrovic, P. Väljamäe, V. G. H. Eijsink and M. Sorlie, Kinetic Characterization of a Putatively Chitin-Active LPMO Reveals a Preference for Soluble Substrates and Absence of Monooxygenase Activity, *ACS Catal.*, 2021, **11**, 11685–11695.
104 L. Rieder and M. Sorlie, Recent Advances in Understanding LPMO Catalysis, *Biochemistry*, 2023, **62**, 3170–3172.